JOURNAL OF GEOPHYSICAL RESEARCH: SPACE PHYSICS, VOL. 118, 4289–4297, doi:10.1002/jgra.50421, 2013

Investigation of the interhemispheric asymmetry in reverse convection near solstice during northward interplanetary magnetic field conditions using MHD simulations

F. D. Wilder,[1] S. Eriksson,[1] and M. Wiltberger[2]

Received 28 April 2013; revised 29 May 2013; accepted 25 June 2013; published 23 July 2013.

[1] The reverse convection potential under northward interplanetary magnetic field (IMF) is significantly larger in the summer ionosphere than in the winter. In this study, we use the Coupled Magnetosphere-Ionosphere-Thermosphere model to simulate a Northern Hemisphere winter event where observations have shown asymmetry in both the reverse convection strength between hemispheres and the magnetic field topology associated with the ionospheric reverse convection cells. We show that a topological asymmetry, in which reconnection between the geomagnetic field and the IMF occurs in the summer hemisphere, first drives the interhemispheric asymmetry in reverse convection strength rather than an interhemispheric asymmetry in ionospheric conductivity. We find a large amount of overdraped open magnetic flux connected to the summer hemisphere that results from this reconnection bypasses the winter hemisphere *x* line and reconnects with the IMF again in the summer hemisphere lobe. This leads to a large amount of circulating lobe flux in the summer hemisphere and stagnant lobe flux in the winter hemisphere, while maintaining a divergence-free field, as well as the weaker reverse convection potential in the winter hemisphere ionosphere.

Citation: Wilder, F. D., S. Eriksson, and M. Wiltberger (2013), Investigation of the interhemispheric asymmetry in reverse convection near solstice during northward interplanetary magnetic field conditions using MHD simulations, *J. Geophys. Res. Space Physics*, *118*, 4289–4297, doi:10.1002/jgra.50421.

1. Introduction

[2] Magnetic reconnection between the interplanetary magnetic field (IMF) and the geomagnetic field is thought to be the primary driver of plasma convection and the transport of energy in the magnetosphere. The magnetic flux transport associated with this convection couples to the polar ionosphere, leading to an ionospheric convection pattern and an associated electrostatic potential, with equipotentials being streamlines of the plasma convection. When the IMF is southward, magnetic reconnection occurs near the subsolar point of the dayside magnetopause, leading to the transport of open flux over the polar regions in the antisunward direction. Some of this open flux reconnects again in the tail, driving sunward return flow in the magnetosphere on closed field lines. This results in an ionospheric convection pattern consisting of two cells with antisunward flow over the polar cap and sunward return flow in the auroral zones [*Dungey*, 1961].

[3] When the IMF is northward, it reconnects with the Earth's magnetic field on the nightside of the magnetosphere poleward of the cusp, leading to a four-cell plasma convection pattern in the polar ionosphere [*Dungey*, 1963]. Two of these cells are larger in spatial extent, consisting of antisunward flow at high latitudes and sunward return flow at low latitudes, and are thought to be due to viscous interactions between the solar wind and the magnetospheric plasma [*Axford and Hines*, 1961]. The other two cells are localized, high-latitude "reverse" convection cells, consisting of sunward flow at high latitudes near local noon and antisunward return flow in the morning and afternoon magnetic local time sectors [*Crooker*, 1992]. These reverse convection cells are thought to be associated with reconnection between the IMF and the Earth's magnetic field on the nightside poleward of the cusp [*Crooker*, 1992; *Phan et al*., 2004; *Watanabe et al*, 2005; *Eriksson et al*., 2005]. While the reverse convection is highly localized, it can still have significant impacts on the ionosphere-thermosphere system. For example, *Wilder et al*., [2012a] showed that ionospheric Joule heating in the reverse convection cells could lead to upwelling of neutral gas and equatorward propagating large-scale gravity waves in the high-altitude thermosphere.

[4] One stark difference between reconnection under northward and southward IMF is that there are separate *x* lines between the IMF and the geomagnetic field in each hemisphere under northward IMF, while there is one around the equatorial dayside under southward IMF. Having a separate location for reconnection in each hemisphere can lead to asymmetries in magnetic flux transport during periods around solstice when the Earth has a large dipole tilt. *Crooker* [1992],

[1]Laboratory of Atmospheric and Space Physics, University of Colorado Boulder, Boulder, Colorado, USA.
[2]National Center for Atmospheric Research, Boulder, Colorado, USA.

Corresponding author: F. D. Wilder, Laboratory of Atmospheric and Space Physics, University of Colorado Boulder, Boulder, CO 80303, USA. (frederick.wilder@lasp.colorado.edu)

2169-9380/13/10.1002/jgra.50421

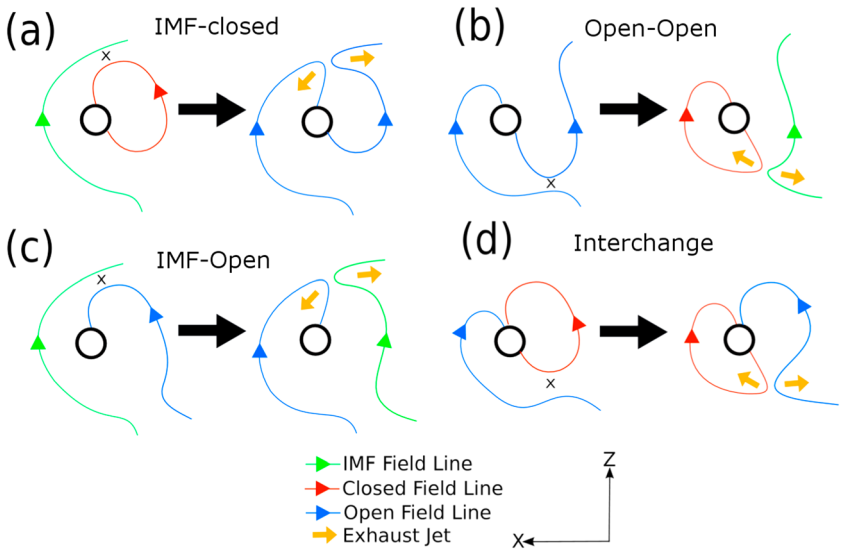

Figure 1. Four reconnection "types" under northward IMF and Northern Hemisphere summer conditions. The magnetic field lines are color coded as follows: green is IMF, red is magnetospheric closed, and blue is magnetospheric open/lobe. The letter *x* between antiparallel fields represents the *x* line (perpendicular to the *x*–*z* plane), and the orange arrows indicate the direction of the J × B force in the reconnection exhaust jet. Adapted from *Watanabe and Sofko* [2009].

as well as *Watanabe et al.* [2005], suggested that near solstice, direct magnetic merging between the IMF and the nightside magnetospheric field only occurs in the summer hemisphere leading to open field lines connecting to the summer polar cap which drape over the dayside, where they can reconnect with nightside magnetospheric field lines in the winter hemisphere.

[5] *Watanabe and Sofko* [2009] outlined four reconnection scenarios that can occur under northward IMF near solstice, which are summarized in Figure 1. Figure 1a shows the IMF reconnecting with a closed nightside field line in the summer hemisphere, resulting in two open field lines: one which drapes from the summer hemisphere polar cap over the dayside magnetosphere and a winter hemisphere lobe field line. This reconnection type will be referred to herein as "IMF-closed." The overdraped field line can then merge with a winter hemisphere lobe field line, as in Figure 1b, resulting in a dayside closed field line, and an IMF field line which is transported with the solar wind away from the magnetosphere. This reconnection type will be referred to as "open-open." A slightly more complex interaction can also occur, as shown in Figures 1c and 1d. Figure 1c shows the IMF reconnecting with a summer hemisphere lobe field line ("IMF-open" reconnection), leading to an overdraped summer open field line. This field line could then reconnect with a winter hemisphere lobe field line (open-open) or be swept back around to the tail, where it can reconnect with the IMF again. This leads to circulation on open field lines in the summer ionosphere, called "lobe cell" circulation [*Reiff and Burch*, 1985; *Watanabe et al.*, 2005]. Additionally, the overdraped field line can reconnect with a closed nightside field line in the winter hemisphere, leading to a closed dayside field line and a summer lobe field line, as in Figure 1d. The reconnection shown in Figure 1d, sometimes referred to as "interchange" reconnection [*Watanabe and Sofko*, 2009], can lead to circulation on closed field lines in the winter ionosphere, referred to as "reciprocal cell" convection [*Watanabe et al.*, 2005]. *Watanabe et al.* [2006] used data from the Super Dual Auroral Radar Network (SuperDARN) and the Defense Meteorological Satellite Program (DMSP) to demonstrate the existence of lobe and reciprocal cells for several case studies.

[6] Hemispheric asymmetries under northward IMF have been investigated empirically using the electrostatic potential across the reverse convection cells, Φ_{RC}. For example, *Wilder et al.* [2009, 2010] found that Φ_{RC} was stronger in the summer hemisphere than the winter hemisphere. This seasonal asymmetry was opposite to the asymmetry in the viscous convection, as well as the two-cell pattern under southward IMF, where the potential was larger in the winter hemisphere. *Wilder et al.* [2011] investigated an event on 5 December 2004, where SuperDARN radars observed reverse convection simultaneously in both hemispheres. In addition to observing that the sunward portion of the reverse convection cells were 700–800 m /s faster in the summer hemisphere than in the winter, they also observed evidence of lobe cell convection in the summer hemisphere and reciprocal cell convection in the winter hemisphere, leading to the hypothesis that the seasonal asymmetry could be driven by magnetic field topology and magnetospheric flux transport as opposed to hemispheric asymmetries in ionospheric conductivity.

[7] The present study builds upon the investigation performed by *Wilder et al.* [2011]. The Coupled Magnetosphere-Ionosphere-Thermosphere (CMIT) model [*Wiltberger et al.*, 2004] is used to simulate the 5 December 2004 event based on solar wind conditions. The magnitude of the sunward magnetospheric flow associated with reconnection in each hemisphere is compared, as well as the electrostatic potential in the northern and southern polar ionospheres. Additionally, large-scale flux transport and magnetic field topology are investigated to determine if the polar cap

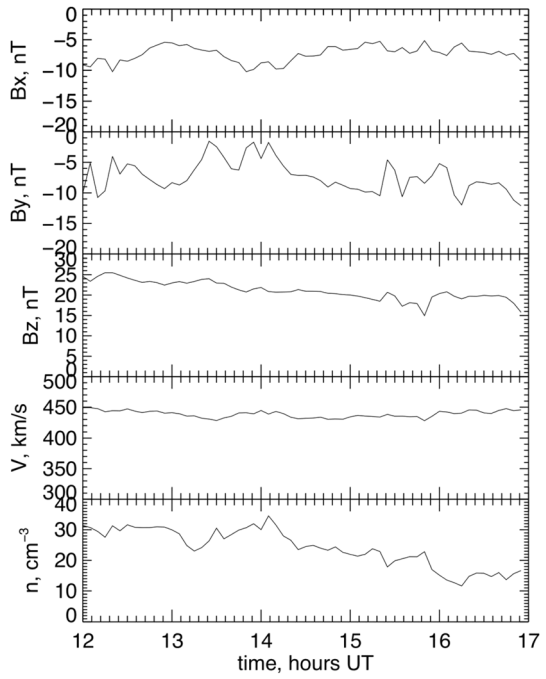

Figure 2. OMNI IMF and solar wind conditions for 5 December 2004. Conditions have been propagated to 17 Re, and the IMF vector is given in geocentric solar magnetospheric (GSM) coordinates.

potential asymmetry is driven by magnetospheric topology unique to northward IMF conditions.

2. Solar Wind Conditions

[8] Figure 2 shows time series of IMF and solar wind conditions propagated to 17 Re and obtained from the OMNI database [*King and Papitashvili*, 2005] for the afternoon of 5 December 2004. During this period, the solar wind speed was nominal at approximately 450 km/s and the IMF was steadily northward at greater than 20 nT for most of the interval. Additionally, there was fluctuating negative IMF B_y and a negative IMF B_x, which will also impact the field topology in the magnetosphere. The negative B_y component can skew the magnetospheric sash in the *y*-*z* plane toward dawn in the Northern Hemisphere and dusk in the Southern Hemisphere [*Siscoe et al*., 2001; *Eriksson and Rastätter*, 2013]. Further, the negative B_x component can partially offset the effects of the dipole tilt during northern winter. Regardless, analysis by *Wilder et al*. [2011] suggested that this effect should be minimal compared to the dipole tilt and northward IMF.

[9] The present study will focus on the interval between 13:00 and 15:00 UT. During this period, the SuperDARN radars had line-of-sight directions approximately along the sunward portion of the reverse convection in both hemispheres and observed large asymmetries in plasma convection speed and Φ_{RC} [*Wilder et al*., 2011]. Additionally, the DMSP F13 satellite passed through the reverse convection cells in each hemisphere [*Wilder et al*., 2011], allowing investigation of the field topology using the SSJ/4 particle detectors [*Hardy et al*., 1984]. Therefore, this interval provides an excellent opportunity to compare simulation results with observations.

3. Results From the Coupled Magnetosphere-Ionosphere-Thermosphere Model

[10] In order to investigate the magnetospheric configuration and resulting ionospheric convection, the present study uses the Coupled Magnetosphere-Ionosphere-Thermosphere (CMIT) model [*Wiltberger et al*., 2004; *Wang et al*., 2004]. CMIT uses the Lyon-Fedder-Mobarry (LFM) MHD code [*Lyon et al*., 2004] coupled with the National Center for Atmospheric Research, Boulder, Colorado Thermosphere-Ionosphere Electrodynamics General Circulation Model (TIE-GCM) [*Richmond et al*., 1992]. The TIE-GCM is driven by precipitation and electric potentials from the LFM magnetosphere-ionosphere coupler (MIX) [*Merkin and Lyon*, 2010] and feeds back to the MIX module through conductivities and neutral winds. This setup is optimal for the present study, as it allows for a first-principles investigation of both the magnetosphere and ionosphere-thermosphere systems as well as more realistic ionospheric conductance patterns. In this study, the CMIT model was run using the NASA Community Coordinated Modeling Center (CCMC). Solar wind and IMF conditions from the Advanced Composition Explorer (ACE) satellite [*Stone et al*., 1997] were used to drive the model, and the F10.7 flux was set at 93×10^{-22} $Wm^{-2}Hz^{-2}$. The dipole tilt was −26° at the beginning of the run at 0:00 UT on 5 December 2004 and varied between −13° and −18° during the 12:00–15:00 UT interval. We note that in the particular study used here, the OMNI data in Figure 2 were specified by ACE data.

3.1. Hemispheric Asymmetry in Sunward Magnetospheric Flow Channels and Reverse Convection in the Ionosphere

[11] Figure 3 shows an *x*–*z* solar magnetic (SM) magnetospheric cut plane with *y* = 0 Re at 14:00 UT. The SM coordinate system is similar to GSM but rotated about the *y* axis by the dipole tilt angle. This allows for more straightforward investigation of hemispheric asymmetries in sunward flow at high latitudes. The color contours show the *x* component of the magnetospheric plasma velocity calculated by CMIT,

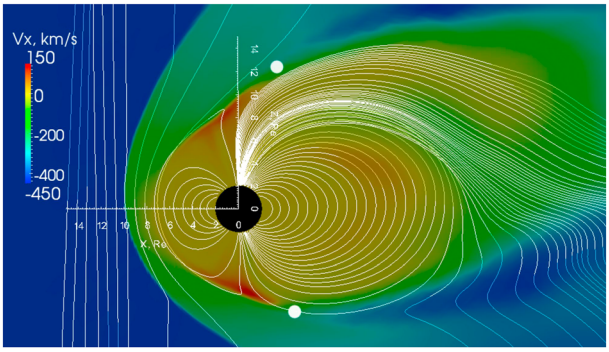

Figure 3. The *x*–*z* SM cut plane with *y* = 0 Re at 14:00 UT showing the *x* component of plasma velocity calculated by the LFM MHD code, with positive values being sunward. White lines indicate 75 3-D magnetic field lines traced from evenly spaced seed points along a line at *z* = −1 Re, *y* = 0 Re from *x* = −50 to 15 Re. White dots are placed on the magnetopause between the oppositely directed reconnection jets and signify the approximate location of the *x* line.

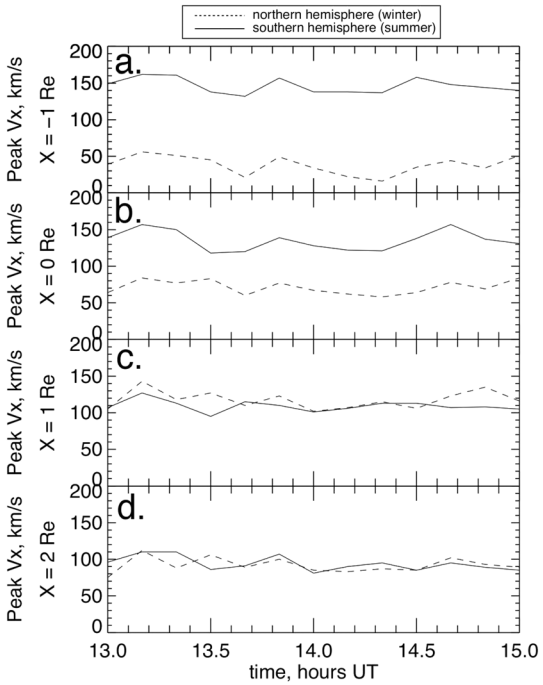

Figure 4. Time series of the peak sunward velocity in each hemisphere at (a) $x = -1$ Re, (b) $x = 0$ Re, (c) $x = 1$ Re, and (d) $x = 2$ Re SM. The dashed and solid lines are the time series for the Northern and Southern Hemispheres, respectively.

with positive being sunward. Seventy-five 3-D field lines have also been traced with seed points evenly spaced along the line in the plane at $z = -1$ Re from $x = -50$ to 15 Re.

[12] Several important features are apparent from Figure 3. First, evidence of highly bent field lines associated with x line geometry is apparent on the dayside near $x = 0$ and $z \sim \pm 9$ Re, which is expected under northward IMF. Additionally, regions of enhanced sunward flow are seen near the x line in each hemisphere, with sunward flow in the Northern Hemisphere reaching 108 km/s and in the Southern Hemisphere reaching 119 km/s. This flow is the dayside portion of the reconnection exhaust and tends to couple to fast sunward flows in the ionosphere [*Eriksson et al*., 2005; *Wilder et al*., 2012b]. The nightside portion of the exhaust can also be seen, with enhanced antisunward flow. For reference, white dots indicate the x lines between the sunward and antisunward exhausts in each hemisphere. Finally, it is worth noting that all of the lobe flux traced in the magnetotail that was traced in this $y = 0$ plane is connecting to the Northern Hemisphere and not the Southern Hemisphere.

[13] In order to investigate the variability of the sunward portion of the reconnection exhaust in each hemisphere, Figure 4 shows time series of the peak sunward flow in the y-z plane at $x = -1$, 0, 1, and 2 Re SM, calculated at 15 min intervals. These peak flows were found by extracting the maximum positive x component of the plasma velocity inside the reconnection exhaust at the three x values. At $x = -1$ and 0 Re, there is a significant asymmetry between the peak flow in the Northern and Southern Hemispheres, with the flow in the Southern Hemisphere being faster by approximately 100 km/s, which would correspond to an asymmetry of a few hundred meters per second in the ionosphere if quasi-equipotential field lines and an ionospheric field strength of 45,000 nT are assumed. At $x = 1$ and 2 Re, the velocities in each hemisphere are comparable, with the flow in the Northern Hemisphere sometimes exceeding that in the Southern Hemisphere but this time on the order of 10–20 km/s. This seems to imply that the jet is skewed further along the positive x axis in the SM coordinate system in the Northern Hemisphere, which is consistent with what is expected under northern winter solstice conditions. Because the Northern Hemisphere is tilted away from the Sun-Earth line due to the dipole tilt, it is likely that overdraped magnetic field lines connected to the Southern Hemisphere will not be able to reconnect with the Northern Hemisphere lobe field as far down tail as the IMF can reconnect with the Southern Hemisphere lobe. It is also worth noting that while the sunward magnetospheric flow is consistently faster over a wider spatial range in the Southern Hemisphere, the hemispheric asymmetries of the peak flow at $y = 0$ (such as in Figure 3) are less dramatic. Similar results were observed by *Wilder et al*. [2011], who found that the average reverse convection

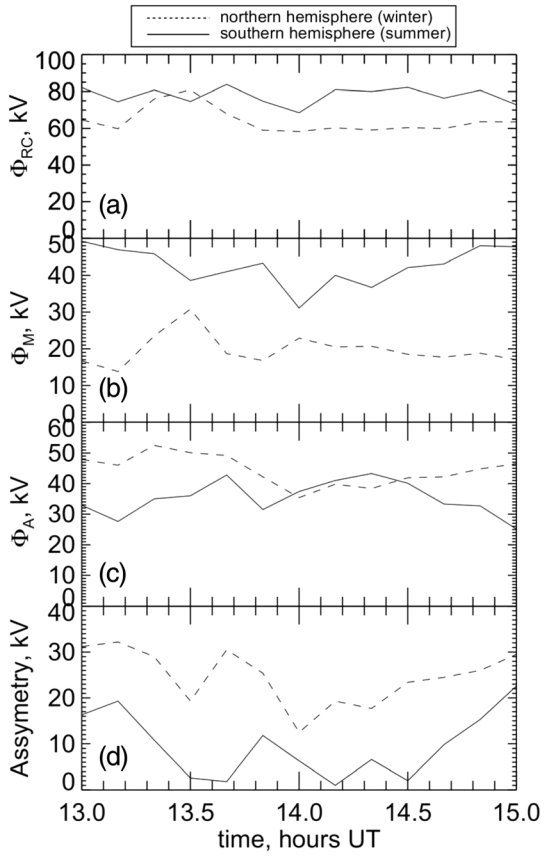

Figure 5. Time series of polar ionospheric potential extrema in each hemisphere: (a) The electrostatic potential drop across the reverse convection cell, Φ_{RC}, (b) the electrostatic potential of the morning reverse convection cell, Φ_M, (c) the electrostatic potential of the afternoon reverse convection cell, Φ_A, and (d) the asymmetry in magnitude between the afternoon and morning potential extrema. The dashed and solid lines are the time series for the Northern and Southern Hemispheres, respectively.

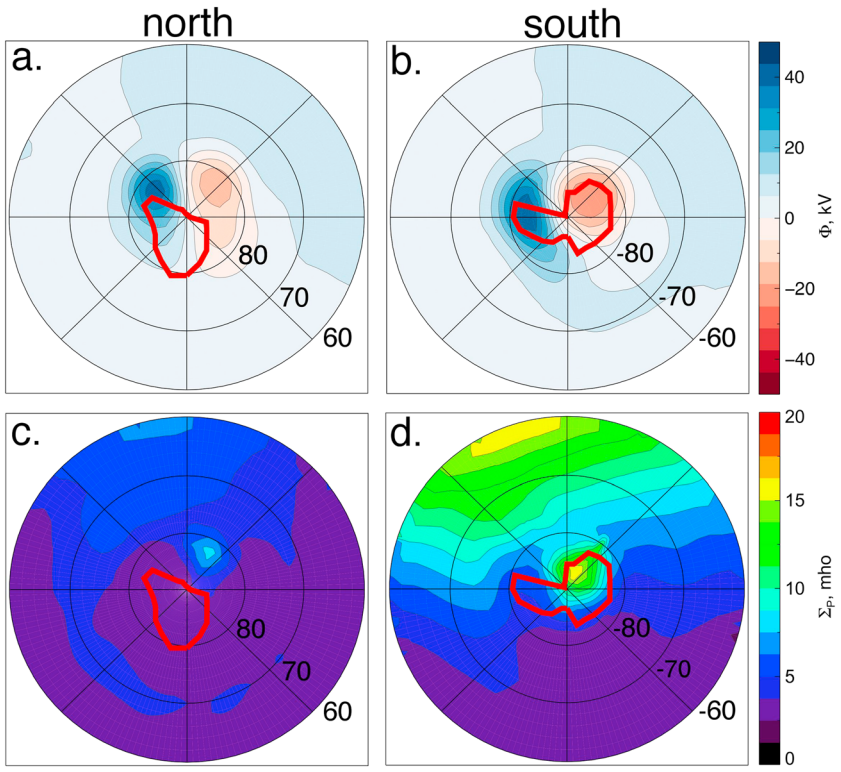

Figure 6. Ionospheric polar cap potential patterns in the (a) Northern and (b) Southern Hemispheres as well as height-integrated Pedersen conductance in the (c) Northern and (d) Southern Hemispheres calculated by the CMIT model at 14:00 UT. The solid red line indicates the polar cap boundary. MLT noon is at the top of the page.

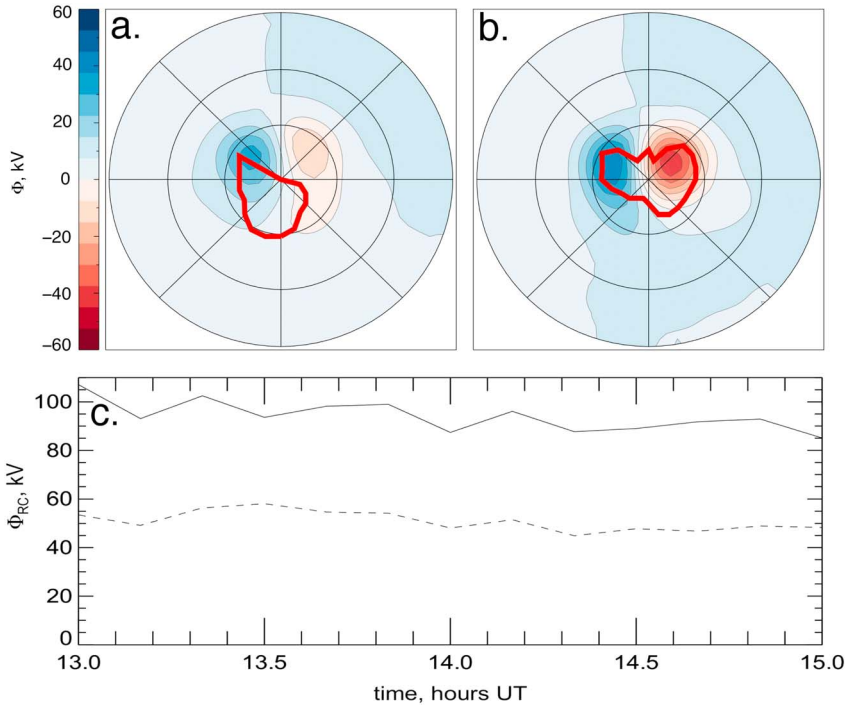

Figure 7. Ionospheric polar cap potential patterns in the (a) Northern and (b) Southern Hemispheres LFM model at 14:00 UT with fixed ionospheric Pedersen conductance of 5 mho in each hemisphere. Maps are given in the same format as Figures 6a and 6b. (c) A time series of the reverse convection potential for the constant conductance LFM run over the same interval as Figure 5. The dashed and solid lines are the Northern and Southern Hemispheres, respectively.

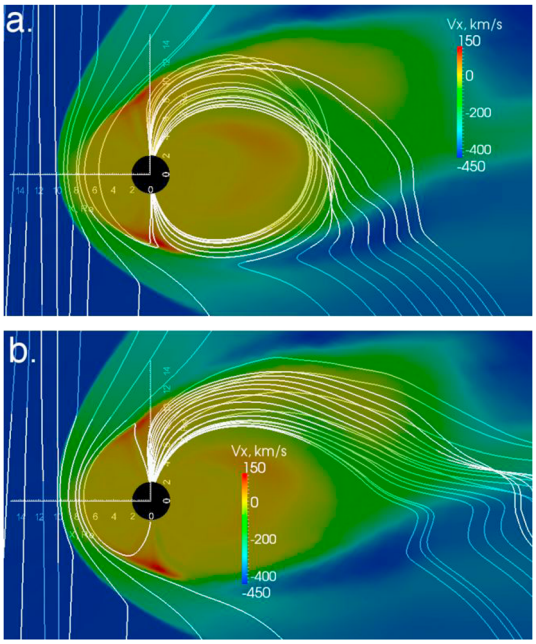

Figure 8. The x–z SM cut planes showing the x component of the plasma velocity, as well as 3-D magnetic field lines. (a) Field lines are traced from 30 evenly spaced seed points along the line at $y = 0$ Re, $z = -7$ Re from $x = -30$ to 20 Re, which intersects the sunward flow channel in the Southern Hemisphere. (b) Field lines are traced from 30 evenly spaced seed points along the line at $y = 0$ Re, $z = 8$ Re from $x = -30$ to 20 Re, which intersects the sunward flow channel in the Northern Hemisphere.

in the ionosphere was several hundred m/s faster in the Southern Hemisphere but also observed that in the unbinned radar observations the peak flows were comparable for the two radars with fields of view along the noon meridian. Therefore, while the peak sunward flow in each hemisphere is comparable, fast flows cover a wider spatial range in the southern/summer hemisphere. It is noted that comparing the CMIT results with the SuperDARN observations of reverse convection assumes that the sunward flow in the ionosphere maps to the sunward reconnection exhausts in the magnetosphere [e.g., *Li et al*., 2011].

[14] In addition to investigating magnetospheric sunward flows, the electrostatic potential pattern in the ionosphere can also be investigated. Figure 5 shows time series of the reverse convection potential, Φ_{RC}, the potential magnitude of the morning reverse convection cell, Φ_M, the potential magnitude of the afternoon reverse convection cell, Φ_A, and the asymmetry in potential magnitude between the morning and afternoon reverse convection cells, $||\Phi_A|-|\Phi_M||$. Time series are shown for the Northern and Southern Hemispheres, represented by dashed and solid lines, respectively. To provide context for these time series, Figures 6a and 6b show the ionospheric potential patterns in both hemispheres calculated by the CMIT model at 14:00 UT with the open-closed boundary superposed. The open-closed boundary was calculated by tracing magnetic field lines from ionospheric seed points along 24 different MLT meridians and identifying when the magnetic separatrix in the magnetosphere is crossed. The largest potentials in both the hemispheres are on the reverse convection cells, found at high latitudes.

[15] From the time series in Figure 5, it is apparent that Φ_{RC} in the Southern (summer) Hemisphere is larger than in the Northern (winter) Hemisphere, which is in agreement with past studies of the seasonal variation reverse convection [*Wilder et al*., 2009, 2010, 2011]. Interestingly, the difference between hemispheres is significantly larger in the morning cell than in the afternoon cell. This is also seen in the time series of the asymmetry in potential magnitude between the morning and afternoon cells. In the Northern Hemisphere, the morning cell is consistently weaker in potential than the afternoon cell. What is more striking is the fact that the potential extrema in the morning and afternoon are significantly more asymmetric in the Northern Hemisphere than in the Southern Hemisphere, as shown in the bottom panel of Figure 5. From Figure 6, a portion of the Northern Hemisphere reverse convection circulates entirely on close field lines. The convection cells that circulate on closed field lines are examples of the reciprocal cells described by *Watanabe et al*. [2005]. In comparing the two reverse cells in the Northern Hemisphere, the morning cell is weaker, and a larger portion of it consists of reciprocal cell convection. Although not shown here, we see that reciprocal cells occur in the simulation consistently throughout the 12:00–15:00 UT interval. Additionally, the weaker convection and spatially larger reciprocal cell convection in the morning sector is also consistently observed in the simulation.

[16] Figures 6c and 6d also show the ionospheric height-integrated Pedersen conductance in each hemisphere for the same intervals as Figures 6a and 6b. As described by *Wiltberger et al*. [2009], these conductance values are calculated using F10.7 flux, assumed electron fluxes in the upward current region, and neutral atmosphere parameters from the TIE-GCM. In comparing the dramatic difference between the winter and summer conductances, one might ascribe the seasonal asymmetry in reverse convection to the conductivity asymmetry. To examine the role of ionospheric conductivity even further, the LFM model was run again for the same event with the same dipole tilt and solar wind conditions, but the Hall and Pedersen conductances were fixed in both hemispheres at 0 and 5 mho, respectively.

[17] Figures 7a and 7b show the polar cap potential pattern and open-closed boundary for the constant conductance run in the Northern and Southern Hemispheres, respectively. The open-closed boundaries are comparable to those in Figure 6 with lobe cell circulation in the Southern Hemisphere and reciprocal cell convection in the Northern Hemisphere. Additionally, Φ_{RC} in the Southern Hemisphere is significantly larger than in the Northern Hemisphere. Figure 7c shows a time series of the reverse convection potential for the constant conductance LFM run during the same time interval as Figure 5. In the Southern (summer) Hemisphere, Φ_{RC} ranges between 85 and 108 kV, while in the Northern (winter) Hemisphere, it ranges between 44 and 59 kV. This is an even larger asymmetry in the run that used FUV and precipitation-driven conductances, where Φ_{RC} in the summer ranged between 72 and 84 kV, while in the winter it ranged between 58 and 81 kV. Therefore, in the run with TIE-GCM conductances, the low-conductivity conditions seem to increase the potential in the winter hemisphere, while the high-conductivity conditions seem to decrease

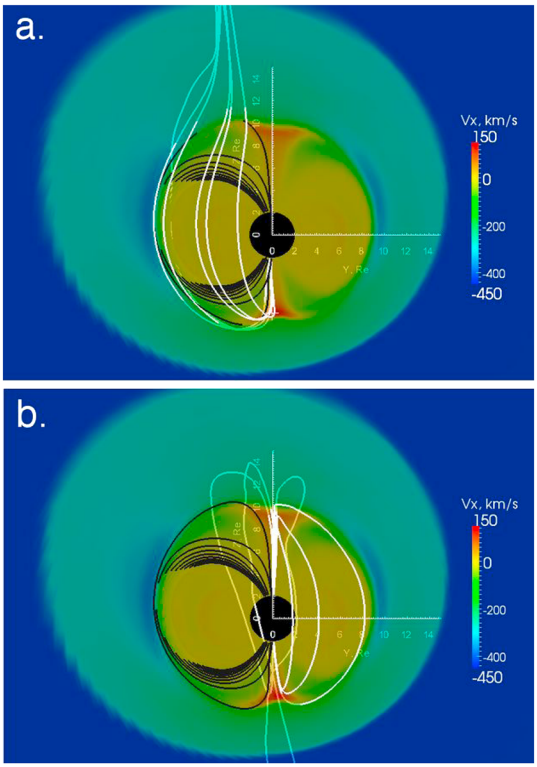

Figure 9. The *y*-*z* SM cut planes showing the *x* component of the plasma velocity and 3-D magnetic field lines. White field lines are traced from six evenly spaced seed points within a 1 Re sphere, centered at (a) $z = -7$ Re and (b) $z = 9$ Re, which corresponds to the sunward flow channel in the Southern and Northern Hemispheres, respectively. Black field lines are traced from 10 evenly spaced seed points along the line at $x = 0$ Re, $z = 5$ Re from $y = -9.9$ to -5 Re.

the potential in the summer hemisphere. Therefore, it is likely that another factor, such as hemispheric asymmetries in the large-scale magnetic flux transport, drives the asymmetry in Φ_{RC} between hemispheres.

3.2. Magnetic Field Topology and Associated Flux Transport

[18] Figure 8a shows an *x*–*z* SM cut plane at $y = 0$ Re of the *x* component of the magnetospheric plasma velocity at 14:00 UT. Field lines are traced using the algorithm used for Figure 3, except with 30 seed points that are evenly spaced along the line at $y = 0$ Re, $z = -7$ Re from $x = -30$ to 20 Re, which intersects the sunward flow channel in the Southern Hemisphere. The *x* line field geometry is seen in the Southern Hemisphere associated with the sunward exhausts on the dayside. The region of peak sunward flow in the Southern Hemisphere corresponds with highly bent open field lines which drape over the dayside where they may be antiparallel with both Northern Hemisphere closed and lobe field lines. Additionally, like in Figure 3, a significant amount of Northern Hemisphere lobe magnetic flux is seen in the tail.

[19] To investigate the topology associated with the Northern Hemisphere *x* line, Figure 8b shows the same *x*–*z* cut plane as Figure 8a, except the 30 seed points are now evenly spaced along the line at $y = 0$ Re, $z = 9$ Re from $x = -30$ to 20 Re, which intersects the sunward flow channel in the Northern Hemisphere. In this case, the Northern Hemisphere sunward exhaust is associated with a closed dayside field line. Again, a significant amount of Northern Hemisphere lobe flux is observed. This suggests that the reconnection in the Northern Hemisphere may be largely associated with reclosing of overdraped open field lines which connect to the Southern Hemisphere polar cap or open-open reconnection from Figure 1.

[20] In order to understand the effect of the negative IMF B_y component on the magnetic topology for this event, Figure 9 shows *y*-*z* SM cut planes with $x = 0$ Re of the *x* component of magnetospheric velocity calculated by the CMIT model at 14:00 UT. Figure 9a shows two sets of magnetic field lines. The black field lines are closed field lines calculated using 10 evenly spaced seed points along line at $x = 0$ Re, $z = 5$ Re from $y = -9.9$ to -5 Re. The white field lines are traced using seven evenly spaced seed points within a 1 Re radius sphere centered at $x = 0$, $y = 0$, $z = -7$ Re and are therefore connected to the Southern Hemisphere sunward flow channel. Portions of the field lines that are dull colored are behind the cut plane. The field lines associated with this flow channel are open and are draped over the dayside. Additionally, the overdraped field lines are skewed toward the Northern Hemisphere dawn sector, due to the negative IMF B_Y component. This was predicted by *Wilder et al.* [2011] based on observed field topology along the spacecraft track of DMSP F13. This implies that interchange reconnection, as in Figure 1d, is more likely to happen in the Northern Hemisphere dawn sector for this event, leading to the larger amount of circulation on closed field lines seen in the morning reverse convection cell as compared to the afternoon reverse cell in Figure 6. Additionally, the overdraped field lines in Figure 9a extend tailward behind the plane, which suggests that some of these field lines bypass the Northern Hemisphere *x* line. This could help explain why the reverse convection potential is weaker in the Northern Hemisphere as less flux is reconnecting.

[21] Figure 9b shows the same velocity cut plane as Figure 9a, but with different magnetic field lines. The black field lines on the dawn flank are the same as in Figure 8a, but the white field lines are traced using seven evenly spaced seed points within a 1 Re radius sphere centered at $x = 0$, $y = 0$, $z = 9$ Re and are therefore connected to the Northern Hemisphere sunward flow channel. Again, portions of the field lines that are dull colored are behind the cut plane. In this case, the model shows closed dayside field lines which are highly bent in the Northern Hemisphere and are likely associated with reconnection such as in Figures 1 b and 1d. The open field lines in Figure 9b appear to be lobe field lines behind the cut plane, which is consistent with the large amount of lobe flux in the Northern Hemisphere seen in Figures 3 and 8.

4. Discussion

[22] The field topology shown in Figures 6–9 can be used to explain both the hemispheric and morning/afternoon asymmetries in Φ_{RC} seen in the simulation. When the IMF encounters the Earth, it reconnects with the geomagnetic field in the Southern Hemisphere (IMF-closed), leading to overdraped field lines connected to the southern polar cap (Figures 8a and 9a) and lobe field lines connected to the northern polar cap (Figures 8b and 9b). The overdraped field

lines are skewed toward dawn where they can reconnect with either Northern Hemisphere lobe flux (open-open) or closed field lines (interchange). Another alternative is for the overdraped field lines to circle around the Earth and become lobe field lines connected to the southern polar cap. Here they can reconnect with the IMF again, becoming overdraped field lines (IMF-open).

[23] The simulation results presented here suggest that on 5 December 2004, a large amount of the open flux that connected to the southern (summer) polar cap was in constant motion, following the sequence given by Figures 1a and 1c. This led to large amounts of circulation on open field lines in both reverse convection cells in Figure 6. Because the overdraped open flux was skewed toward the dawn sector, most of the merging between overdraped field lines and closed magnetospheric field lines (Figure 1d) occurred in the dawn sector, leading to a morning cell in the Northern Hemisphere that circulated largely on closed field lines. The electric potential in the morning cell of the northern polar cap potential pattern was typically weaker, probably because many of the overdraped summer field lines bypassed the *x* line and convected tailward. Thus, we see a strong lobe cell in the Southern Hemisphere morning sector and a weak reciprocal cell in the Northern Hemisphere morning sector. Because the largest asymmetry between the Northern and Southern Hemispheres reverse convection potential lies in the morning cell, it is likely that the weaker potential in the winter hemisphere is due to the amount of overdraped flux tubes from the Southern Hemisphere bypassing the *x* line in the Northern Hemisphere.

[24] With regard to open field lines connected to the Northern Hemisphere, Figure 6 shows that there is a large amount of open flux centered around regions where the ionospheric electrostatic potential magnitude, and therefore plasma velocity, is very small. This implies that there is a significant amount of stagnant lobe flux connected to the Northern Hemisphere polar cap, which explains the large amount of Northern Hemisphere lobe flux seen in the field line traces in Figures 3, 8, and 9. The sunward convection crossing the open-closed boundary from the open side of Figure 6a implies that some of the Northern Hemisphere lobe flux is closed when it reconnects with overdraped field lines connected to the Southern Hemisphere (open-open). This closed dayside flux circulates tailward, where it can reconnect again with the IMF in the Southern Hemisphere (IMF-closed), as seen in the flow across the open-closed boundary on the nightside of the afternoon cell in Figure 6a. We note that the topology outlined here does not violate the divergence-free condition of the magnetic field. The open magnetic flux into the Northern Hemisphere is the same as the open flux out of the Southern Hemisphere—what drives the asymmetry between the associated potentials is the fact that much of the open flux connected to the Southern Hemisphere is in constant motion, while much of the open flux connected to the Northern Hemisphere is largely stagnant.

[25] The convection and topology outlined above is also observed in ionospheric data sets. For example, Figure 9 from *Wilder et al*. [2011] showed SuperDARN patterns averaged over two DMSP passes through each hemisphere during the afternoon of 5 December 2004. Additionally, they calculated the open-closed field line boundary (OCFLB) boundary using SSJ/4 precipitating particle data. The OCFLB and convection characteristics they observed are very similar to those shown in Figures 6 and 7. They found evidence of circulation on open field lines in both reverse convection cells in the Southern Hemisphere, with clear evidence of a strong lobe cell in the morning sector. In the Northern Hemisphere, there was a weak reciprocal cell in the morning sector and a convection cell with two crossings of the open-closed boundary in the afternoon sector. Therefore, it appears that the continuous motion of summer hemisphere open flux that bypasses the morning sector *x* line, coupled with stagnant lobe flux in the Northern Hemisphere, leads to the stronger Φ_{RC} and plasma convection in the Southern (summer) Hemisphere.

5. Conclusion

[26] The present study simulated an event with an observed asymmetry between the reverse convection potential in the winter and summer hemisphere. The conceptual reconnection types outlined by *Watanabe and Sofko* [2009] were used as a framework to understand how large-scale flux transport in the magnetosphere can impact the asymmetries between the ionospheric convection in each hemisphere. It was demonstrated that the weaker Φ_{RC} in the winter hemisphere was due to the dawn cell being driven largely by reconnection between closed field lines and open field lines connected to the summer polar cap that draped over the dayside. Because a large amount of this overdraped flux likely bypassed the *x* line and convected with the magnetosheath plasma tailward, less flux was reconnected in the winter hemisphere dawn sector, leading to a weakened reciprocal cell in the ionosphere. This, in turn, led to a reduced reverse convection potential in the winter hemisphere. In the absence of a significant IMF B_x or B_y component, it is possible that both convection cells in the winter hemisphere could be weakened by the fact that much of the overdraped flux from the summer hemisphere bypasses the Northern Hemisphere *x* line. This could explain the statistically observed asymmetry between the winter and summer Φ_{RC} that appears to be opposite to the trend observed for the polar cap potential under southward IMF conditions [*Wilder et al*., 2009, 2010].

[27] The present study contributes to the ongoing effort to predict ionosphere-thermosphere dynamics under nonsouthward IMF conditions by investigating the magnetospheric driver of intense convection at high latitudes on the dayside. We find that the framework provided by past studies of magnetic reconnection and magnetic field topology under northward IMF [e.g., *Crooker*, 1992; *Watanabe et al*., 2005, 2006; *Watanabe and Sofko*, 2009] explains hemispheric asymmetries in reverse convection that may not be caused by seasonally varying ionospheric conductivity. Because this framework is captured by physics-based models such as the CMIT model shown here, it should be useful in predicting the behavior of the magnetosphere-ionosphere-thermosphere system under northward IMF.

[28] **Acknowledgments.** F.D.W.'s efforts were supported by the National Science Foundation Atmospheric and Geospace Sciences Postdoctoral Research Fellowship. S.E. was supported by NSF under grant AGS-1144154. The National Center for Atmospheric Research is supported by the National Science Foundation. Simulation results have been provided by the Community Coordinated Modeling Center at Goddard Space Flight Center through their public Runs on Request system (http://ccmc.gsfc.nasa.gov). The CCMC is a

multiagency partnership between NASA, AFMC, AFOSR, AFRL, AFWA, NOAA, NSF, and ONR.

[29] Masaki Fujimoto thanks Nozomu Nishitani and another reviewer for their assistance in evaluating this paper.

References

Axford, W., and C. Hines (1961), A unifying theory of high-latitude geophysical phenomena and geomagnetic storms, *Can. J. Phys.*, *39*, 1433.

Crooker, N. (1992), Reverse convection, *J. Geophys. Res.*, *97*(A12), 19,363–19,372.

Dungey, J. W. (1961), Interplanetary magnetic field and the auroral zones, *Phys. Rev. Lett.*, *6*, 47–48.

Dungey, J. (1963), The structure of the exosphere or adventures in velocity space, in *Geophysics, The Earth's Environment*, edited by C. DeWitt, J. Hieblot and A. Lebeau, p. 505, Gordon and Breach, New York.

Eriksson, S., and L. Rastätter (2013), Alfvén Mach number and IMF clock angle dependencies of sunward flow channels in the magnetosphere, *Geophys. Res. Lett.*, *40*, 1257–1262, doi:10.1002/grl50307.

Eriksson, S., et al. (2005), On the generation of enhanced sunward convection and transpolar aurora in the high latitude ionosphere by magnetic merging, *J. Geophys. Res.*, *110*, A11218, doi:10.1029/2005JA011149.

Hardy, D., H. Yeh, L. Schmitt, T. Schumaker, M. Gussenhoven, A. Huber, F. Marshall, and J. Pantazis (1984), Precipitating electron and ion detectors (SSJ/4) for block SD/flights 6-10 DMSP satellites: Calibration and data presentation, *Environ. Res. Pap.*, *902*.

King, J. H., and N. E. Papitashvili (2005), Solar wind spatial scales in and comparisons of hourly Wind and ACE plasma and magnetic field data, *J. Geophys. Res.*, *110*, A02209, doi:10.1029/2004JA010804.

Li, W., D. Knipp, J. Lei, and J. Raeder (2011), The relation between dayside local Poynting flux enhancement and cusp reconnection, *J. Geophys. Res.*, *116*, A08301, doi:10.1029/2011JA016566.

Lyon, G. J., J. A. Fedder, and C. M. Mobarry (2004), The Lyon-Fedder-Mobarry (LFM) global MHD magnetosphere simulation code, *J. Atmosph. Sol.-Terr. Phys.*, *66*(15-16), 1333–1350.

Merkin, V. G., and J. G. Lyon (2010), Effects of the low-latitude ionospheric boundary condition on the global magnetosphere, *J. Geophys. Res.*, *115*, 10202, doi:10.1029/2010JA015461.

Phan, T. D., et al. (2004), Cluster observations of continuous reconnection at the magnetopause under steady interplanetary magnetic field conditions, *Ann. Geophys.*, *22*, 2355–2367.

Reiff, P. H., and J. L. Burch (1985), IMF B_Y-dependent plasma flow and Birkeland currents in the dayside magnetosphere: 2. A global model for northward and southward IMF, *J. Geophys. Res.*, *90*(A2), 1595–1609.

Richmond, A. D., E. C. Ridley, and R. G. Roble (1992), A thermosphere/ionosphere general circulation model with coupled electrodynamics, *Geophys. Res. Lett.*, *19*, 601–604.

Siscoe, G. L., G. M. Erickson, B. U. O. Sonnerup, N. C. Maynard, K. D. Siebert, D. R. Weimer, and W. W. White (2001), Magnetospheric sash dependence on IMF direction, *Geophys. Res. Lett.*, *28*(10), 1921–1924, doi:10.1029/2000GL003784.

Stone, E., A. Frandsen, R. Mewaldt, E. Christian, D. Margolies, J. Ormes, and F. Snow (1997), The advanced composition explorer, *Space Sci. Rev.*, *86*, 1–22, 1998.

Wang, W., M. Wiltberger, A. G. Burns, S. C. Solomon, T. L. Killeen, N. Maruyama, and J. G. Lyon (2004), Initial results from the Coupled Magnetosphere-Ionosphere-Thermosphere model: Thermosphere-ionosphere responses, *J. Atmos. Solar-Terr. Phys.*, *66*(15-16), 1425.

Watanabe, M., and G. J. Sofko (2009), The interchange cycle: A fundamental mode of magnetic flux circulation for northward interplanetary magnetic field, *Geophys. Res. Lett.*, *36*, L03107, doi:10.1029/2008GL036682.

Watanabe, M., K. Kabin, G. J. Sofko, R. Rankin, T. I. Gombosi, A. J. Ridley, and C. R. Clauer (2005), The internal reconnection for northward interplanetary magnetic field, *J. Geophys. Res.*, *110*, A06210, doi:10.1029/2004JA010832.

Watanabe, M., G. J. Sofko, D. A. Andre, J. M. Ruohoniemi, M. R. Hairston, and K. Kabin (2006), Ionospheric signatures of internal reconnection for northward interplanetary magnetic field: Observations of "reciprocal cells" and magnetosheath ion precipitation, *J. Geophys. Res.*, *111*, A06201, doi:10.1029/2005JA011446.

Wilder, F. D., C. R. Clauer, and J. B. H. Baker (2009), Reverse convection potential saturation during northward IMF under various driving conditions, *J. Geophys. Res.*, *114*, A08209, doi:10.1029/2009JA014266.

Wilder, F. D., C. R. Clauer, and J. B. H. Baker (2010), Polar cap electric field saturation during interplanetary magnetic field B_Z north and south conditions, *J. Geophys. Res.*, *115*, A10230, doi:10.1029/2010JA015487.

Wilder, F. D., C. R. Clauer, J. B. H. Baker, and P. T. Newell (2011), Interhemispheric observations of dayside convection under northward IMF, *J. Geophys. Res.*, *115*, A10230, doi:10.1029/2011JA016748.

Wilder, F. D., G. Crowley, B. J. Anderson, and A. D. Richmond (2012a), Intense dayside Joule heating during the 5 April 2010 geomagnetic storm recovery phase observed by AMIE and AMPERE, *J. Geophys. Res.*, *117*, A05207, doi:10.1029/2011JA017262.

Wilder, F. D., G. Crowley, S. Eriksson, P. T. Newell, and M. R. Hairston (2012b), Ionospheric Joule heating, fast flow channels, and magnetic field line topology for IMF B_Y-dominant conditions: Observations and comparisons with predicted reconnection jet speeds, *J. Geophys. Res.*, *117*, A11311, doi:10.1029/2012JA017914.

Wiltberger, M., W. Wang, A. G. Burns, S. C. Solomon, J. G. Lyon, and C. C. Goodrich (2004), Initial results from the Coupled Magnetosphere-Ionosphere-Thermosphere model: Magnetospheric and ionospheric responses, *J. Atmos. Solar-Terr. Phys.*, *66*, 1411, doi:10.1016/j.jastp.2004.04.026.

Wiltberger, M., R. S. Weigel, W. Lotko, and J. A. Fedder (2009), Modeling seasonal variations of auroral particle precipitation in a global-scale magnetosphere-ionosphere simulation, *J. Geophys. Res.*, *114*, 01204, doi:10.1029/2008JA013108.